

Quantitative Determination of the Hydrophobicity of Nanoparticles

Guangle Li, Zhenle Cao, Kacie K. H. Y. Ho, and Yi Y. Zuo*

Cite This: *Anal. Chem.* 2022, 94, 2078–2086

Read Online

ACCESS |



Metrics & More

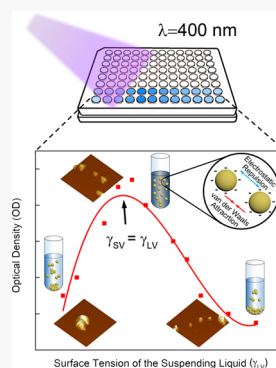


Article Recommendations



Supporting Information

ABSTRACT: The hydrophobicity of nanoparticles (NPs) is one of the most important physicochemical properties that determines their agglomeration state under various environmental conditions. When studying nano–bio interactions, it is found that the hydrophobicity of NPs plays a predominant role in mediating the biological response and toxicity of the NPs. Although many methods have been developed to qualitatively or quantitatively determine hydrophobicity, there is not yet a scientific consensus on the standard of characterizing the hydrophobicity of NPs. We have developed a novel optical method, called the maximum particle dispersion (MPD), for quantitatively characterizing the hydrophobicity of NPs. The principle of measurement of the MPD method lies in the control of the aggregation state of the NPs via manipulating the van der Waals interactions between NPs across a dispersion liquid. We have scrutinized the mechanism of the MPD method using a combination of dynamic light scattering and atomic force microscopy and further verified the MPD method using a completely independent dye adsorption method. The MPD method demonstrated great promise to be developed into an easy-to-use and cost-effective method for quantitatively characterizing the hydrophobicity of NPs.



Hydrophobicity describes the ability of a surface to repel water molecules. The hydrophobicity of an ideal surface is determined by its surface free energy (SFE), which is the excess energy carried by a unit surface area.¹ The SFE is a characteristic physicochemical property of a material that reflects unbalanced intermolecular forces at the surface.² A material with a low SFE typically consists of nonpolar molecules with the van der Waals forces being the predominant intermolecular forces, resulting in primarily hydrophobic properties, such as Teflon and most organic solvents. A material with a high SFE is usually made of polar molecules with metallic or hydrogen bonding being the predominant intermolecular forces, thus showing primarily hydrophilic properties, such as metals and water. Hence, the SFE can be used to quantitatively characterize the hydrophobicity of a material.

Hydrophobicity is one of the most important physicochemical properties of nanoparticles (NPs). It plays a significant role in determining the behavior of nano–bio interactions and the fate of NPs in biological and environmental systems.³ When interacting with biological systems, it has been found that the hydrophobicity of NPs plays a predominant role in mediating the biological response and toxicity of NPs, including the formation of protein and lipid coronas,^{4–6} immune response,^{7,8} cellular uptake,⁹ bioaccumulation, and bioavailability.¹⁰

Compared to bulk materials, characterization and interpretation of the hydrophobicity of NPs are significantly more challenging due to their heterogeneity at the nanoscale and dynamic changes in the environment, e.g., the wetting transition due to surface photosensitivity of NPs.^{11,12} To date, multiple methods have been developed to determine the

hydrophobicity of NPs. These methods can be broadly separated into two categories: qualitative methods, which generally rank the relative hydrophobicity of NPs, and quantitative methods, which determine the SFE of NPs. Figure 1 gives an overview of a few commonly used methods for determining the hydrophobicity of NPs.

Qualitative methods mostly include multiliquid phase partitioning^{13,14} and the dye partitioning method.^{15,16} These methods estimate the hydrophobicity of the NPs by determining the relative affinity between the tested NPs and specific chemicals with known hydrophobicity. For the multiliquid phase partitioning method (Figure 1A), the partitioning coefficient of NPs between two immiscible phases, typically water and octanol, is measured to estimate the relative hydrophobicity of the NPs. For the dye partitioning method (Figure 1B), a specific hydrophobic probe molecule, Rose bengal (RB), is typically used. The relative hydrophobicity of the NPs is determined by plotting the partitioning quotient (PQ) of the dye against the total surface area of the NPs. These qualitative methods are useful for comparing the relative hydrophobicity of a series of NPs measured under the same experimental conditions. Since the results are relative rather than absolute, direct comparison of hydrophobicity data across literatures is not feasible.

Received: September 25, 2021

Accepted: January 3, 2022

Published: January 14, 2022



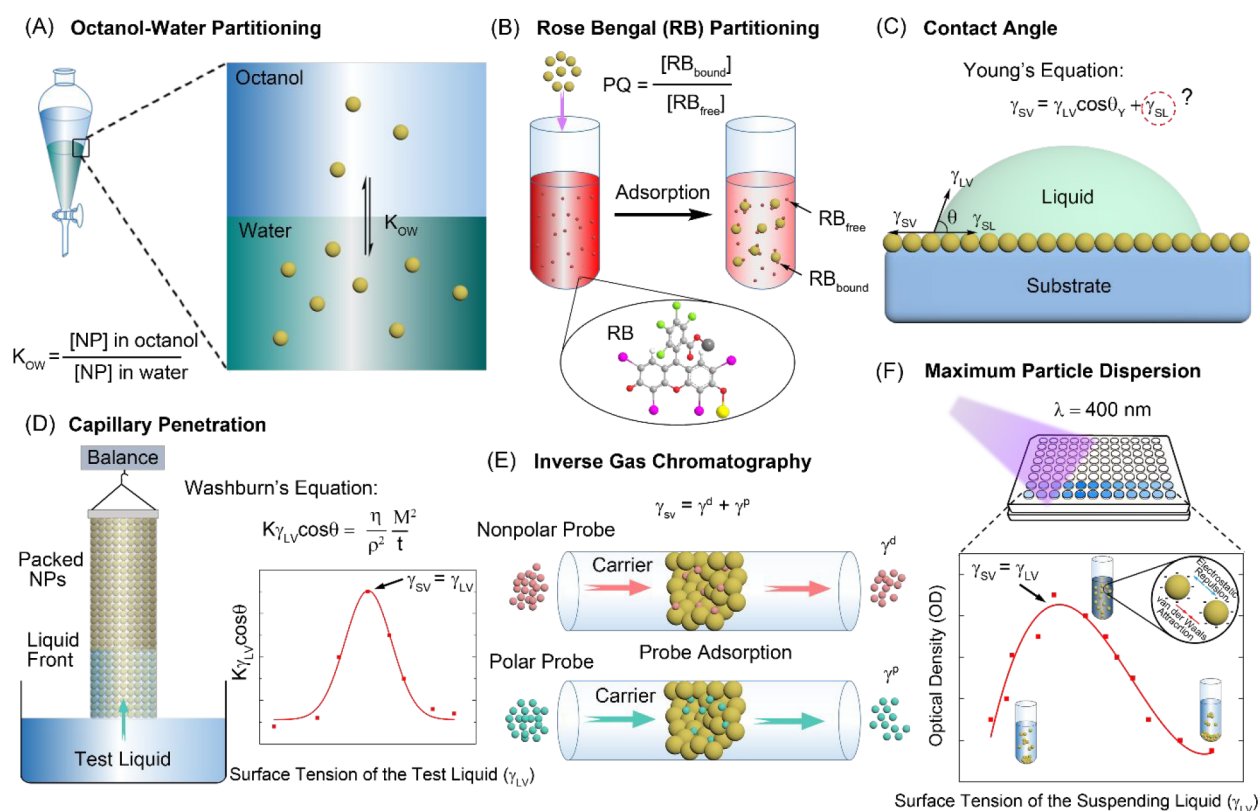


Figure 1. Experimental methods available for determining the hydrophobicity of NPs. (A) The octanol–water partitioning method. The partitioning coefficient (K_{OW}) of NPs between octanol and water is used to determine the relative hydrophobicity of the NPs. (B) The Rose bengal (RB) partitioning method. The relative hydrophobicity of NPs is indicated by the slope of the partitioning quotient (PQ) of the hydrophobic dye, RB, against the total surface area of the NPs. (C) The contact angle method. When used as a qualitative method, the apparent contact angle of a water sessile drop on the NP-coated surface is indicative of the particle hydrophobicity. When used as a quantitative method, the surface free energy (SFE) of NPs (γ_{SV}) can be determined from Young's equation, where two complications are involved. One is the difficulty in determining the Young's contact angle (θ_Y), and another is the uncertainty in calculating the solid–liquid interfacial tension (γ_{SL}) as controversial theories exist. (D) The capillary penetration method. The SFE of NPs is determined from a modified Washburn's equation with a series of liquids of various surface tensions being imbibed into a column packed with the NPs. (E) Inverse gas chromatography. Dispersive (γ^d) and polar (γ^p) components of the SFE are determined by measuring the adsorption of probing gases of different polarities passing the NPs. The total SFE of the NPs is calculated as the sum of individual SFE components. (F) The maximum particle dispersion method. NPs are dispersed in a series of probing liquids of various surface tensions. The surface tension of the liquid in which the NPs are maximally dispersed, determined by an optical density (OD) peak, corresponds to the SFE of the NPs.

Being the most commonly used method for determining hydrophobicity, the contact angle method can be operated either qualitatively or quantitatively.^{14,17–19} When being used as a qualitative method, one determines the apparent contact angle of a water sessile drop on a solid surface coated or packed with particles. The higher the contact angle, the more hydrophobic the particles are. However, the value of the apparent contact angle is generally affected by environmental and measurement conditions, especially by the volume of the water droplet, a phenomena called contact angle hysteresis.²⁰ Hence, results of apparent contact angles reported in different literatures are not directly comparable. When being used as a quantitative method for determining the SFE (Figure 1C), the contact angle method becomes exponentially more complicated, mainly for two reasons. First, it is not an easy task to determine the Young's contact angle (θ_Y), which is a unique angle and only exists for a smooth and homogeneous ideal surface.²⁰ Methods have been developed to circumvent this difficulty, which allow contact angle measurements of individual particles but introduce new uncertainties and complications in sample preparation.²¹ Second, it is theoretically challenging in determining the solid–liquid interfacial

tension (γ_{SL}) used in Young's equation, since controversial theories (Neumann's equation of state²⁰ vs the surface tension component theory²²) exist. In addition to contact angle measurement, a few other methods have been developed for quantitatively determining the SFE of particles, such as capillary penetration (Figure 1D),²³ inverse gas chromatography (Figure 1E),^{24–27} sedimentation volume,²⁸ and solid-surface binding affinity.²⁹ However, none of these methods has been generally accepted as a standard method to study NPs. Thus, there is an urgent need to develop an accurate, easy-to-use, and cost-effective method for quantitatively characterizing the hydrophobicity of NPs.

Recently, we have demonstrated the potential of a proof-of-concept method, called the maximum particle dispersion (MPD) (Figure 1F),³⁰ for determining the SFE of micro- and nanoparticles. The MPD method relies on a novel measurement principle based on controlling the Derjaguin–Landau–Verwey–Overbeek (DLVO) stability of colloidal systems. It can be easily performed with routine optical equipment such as a microplate reader. In the present study, we have scrutinized the mechanism of the MPD method using a combination of dynamic light scattering (DLS) and atomic force microscopy

Table 1. Summary of the Nanoparticles (NPs) Studied

NPs ^a	source	particle morphology and size	hydrodynamic size (nm) ^b	ζ -potential (mV) ^b	measured SFE (mJ/m ²)
TCS-ZnO	JRC, European Commission	nanorods, 59 nm in diameter and 144 nm in length	281 ± 6	-23.7 ± 0.7	21.2 ± 0.4
MWCNT	Strem Chemicals	fibers, 141 nm in diameter and 4 μm in length	1621 ± 570	-35.4 ± 4.5	24.5 ± 0.6
TiO ₂	Sigma-Aldrich	NPs, 23 nm in diameter	1252 ± 38	-43.7 ± 2.9	30.4 ± 1.5
GNP	Strem Chemicals	sheets, 3.6 μm in diameter and 6–8 nm thick	3143 ± 955	-40.5 ± 6.8	30.9 ± 0.8
CeO ₂	Sigma-Aldrich	NPs, 27 nm in diameter	1278 ± 32	-38.9 ± 2.8	35.5 ± 0.9
PST	Thermo Scientific	monodisperse nanospheres, 707 nm in diameter	803 ± 12	-76.7 ± 6.0	36.4 ± 1.4

^aTCS-ZnO NPs, triethoxycaprylsilane-coated zinc oxide nanoparticles; MWCNT, multiwalled carbon nanotubes; TiO₂ NPs, titanium dioxide nanoparticles; GNP, graphene nanoplatelets; CeO₂ NPs, cerium oxide nanoparticles; PST NPs, polystyrene nanoparticles; JRC, joint research center repository of representative industrial nanomaterials; SFE, surface free energy. ^bThe hydrodynamic size and ζ -potential of these NPs were measured in PBS solution (pH 7.4).

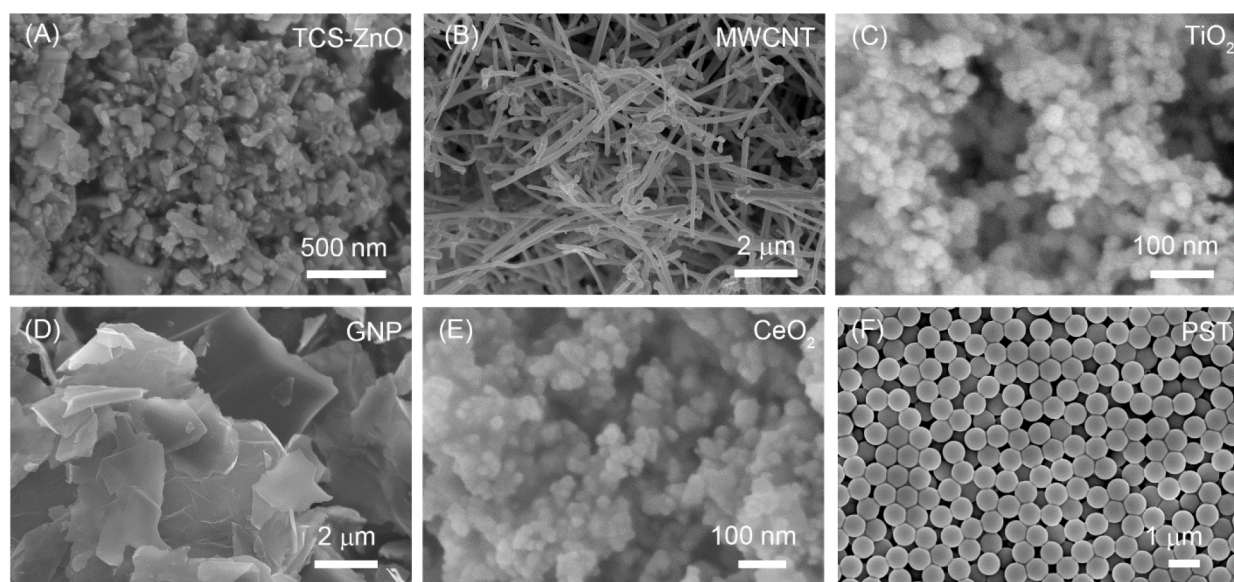


Figure 2. Scanning electron microscopy (SEM) micrographs showing the morphology of the studied nanoparticles (NPs): (A) triethoxycaprylsilane-coated zinc oxide (TCS-ZnO) NPs, (B) multiwalled carbon nanotubes (MWCNT), (C) titanium dioxide (TiO₂) NPs, (D) graphene nanoplatelets (GNP), (E) cerium oxide (CeO₂) NPs, and (F) polystyrene (PST) NPs.

(AFM) and further verified the MPD method with a completely independent method based on dye adsorption. The MPD method shows great promise to be developed into a standard method for characterizing the hydrophobicity of NPs.

EXPERIMENTAL SECTION

Materials. Nanoparticles and solvents were purchased from commercial sources summarized in Table 1 and Table S1. Rose bengal and Nile blue A (NB) were purchased from Sigma-Aldrich (St. Louis, MO). The water used was Milli-Q ultrapure water (Millipore, Burlington, MA) with a resistivity greater than 18 MΩ·cm at room temperature.

Characterization of the NPs. Morphologies of the NPs were characterized by scanning electron microscopy (SEM, Hitachi S-4800, Tokyo, Japan). Primary sizes of the NPs were analyzed with ImageJ. Hydrodynamic size, size distribution, polydispersity index (PDI), and ζ -potentials of the NPs were determined by a Zetasizer Nano ZS (Malvern Panalytical, Malvern, U.K.). Hydrodynamic sizes of all NPs were determined by assuming a spherical shape. The viscosity of water/ethanol mixtures was measured with an Ostwald viscometer (Lambda Scientific System, Miami, FL) at room temperature. The refractive indexes (RI) used for the

measurements were 1.330, 1.360, 1.350, and 1.346 for water, ethanol, and water/ethanol mixtures with surface tensions of 30.4 and 34.8 mJ/m², respectively.³¹ Aggregation states of the NPs were imaged with an Innova atomic force microscope (Bruker, Santa Barbara, CA). Samples were scanned using tapping mode in air by a silicon cantilever with a resonance frequency of 300 kHz and a spring constant of 42 N/m. Images were taken at multiple locations ($n > 3$) to ensure representativeness and reproducibility. Lateral structures of the samples were analyzed, and three-dimensional (3D) renderings were produced using Nanoscope Analysis software.

Maximum Particle Dispersion Method. A trace amount of the NP stock solution was added to a series of probing liquids of 0.5 mL each. There were two sets of probing liquids: a polar liquid set consisting of water/ethanol mixtures, covering the surface tension range from 22.3 mJ/m² (pure ethanol) to 71.4 mJ/m² (pure water), and a nonpolar liquid set consisting of six alkanes ranging from C₅ to C₁₆, covering the surface tension range of 16–27 mJ/m². The density, viscosity, and surface tension of these two sets of liquids were measured, and the results are shown in Figures S5 and S6. After being vortexed, the mixtures were centrifuged at 100–700g for at least 5 min. Subsequently, 160 μL of the supernatant from each

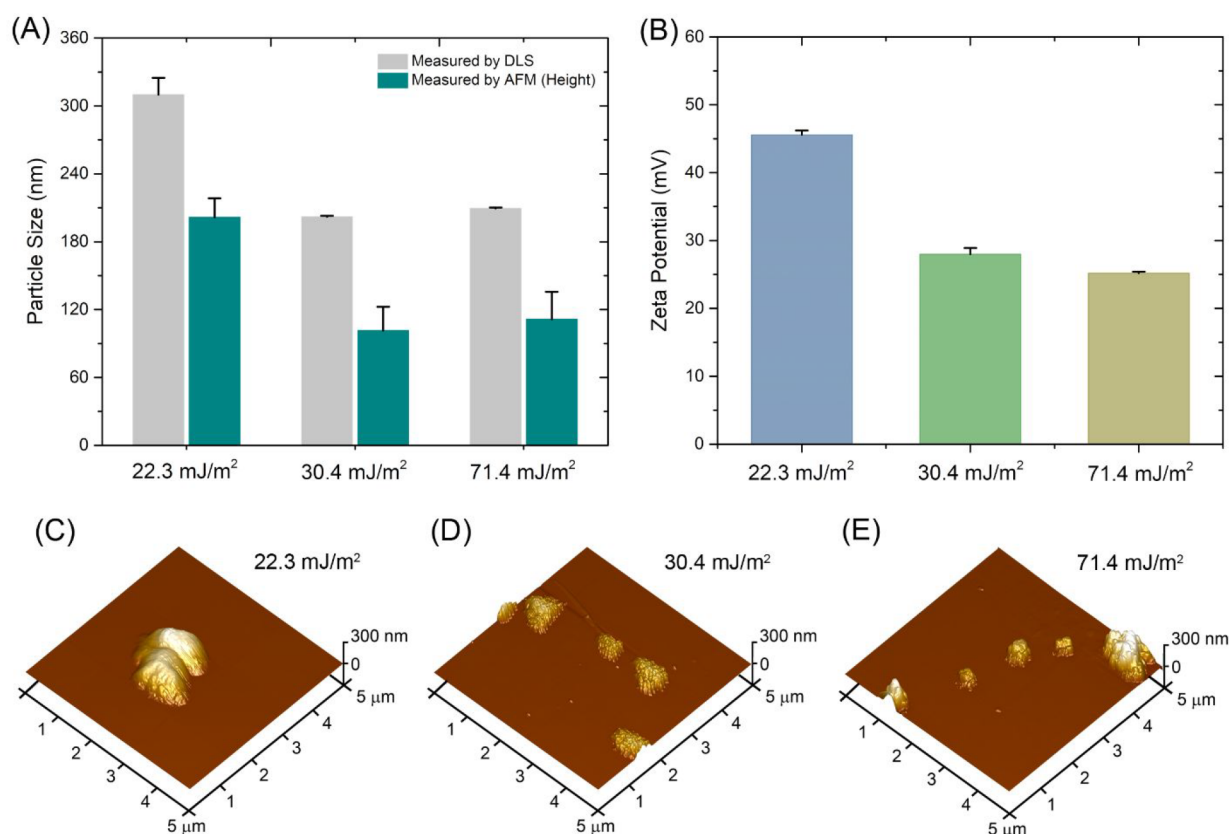


Figure 3. Aggregation state of TiO₂ NPs in three representative probing liquids, i.e., pure ethanol (22.3 mJ/m²), pure water (71.4 mJ/m²), and the ethanol/water mixture in which the TiO₂ NPs are maximally dispersed (30.4 mJ/m²). (A) Hydrodynamic size of the TiO₂ NPs determined with dynamic light scattering (DLS) and the particle size determined with atomic force microscopy (AFM). (B) The ζ -potentials of the TiO₂ NPs in three suspending liquids. (C–E) AFM topographic images of the TiO₂ NPs in three suspending liquids.

suspension was transferred to a 96-well microplate without disturbing the sediment. The optical density (OD) at 400 nm was measured using a microplate reader (Epoch, BioTek, Winooski, VT). The OD value was plotted against the surface tension of the probing liquid, and the SFE of the NPs was determined at the maximum OD value obtained by optimal peak fitting using OriginPro. Each measurement was repeated at least three times, and results are shown as mean \pm standard deviation.

Dye Adsorption Method. The relative hydrophobicity of the NPs was determined using the dye adsorption method. Both the hydrophobic dye, RB, and the hydrophilic dye, NB, were used. A 2 mg/mL dye solution was diluted to 20 μ g/mL using phosphate-buffered saline (PBS) solution at pH 7.4. A series of NP stock solutions at a range of concentrations were added to the dye solution to create an array of suspensions. All suspensions were incubated at room temperature for 3 h and subsequently centrifuged at 16 000g for 1 h. The total surface area of the NPs dispersed in the suspension was calculated from the hydrodynamic size of these NPs determined with DLS, by assuming a spherical shape. The supernatants were collected, and the remaining concentration of the dye molecules in the supernatant was determined with a UV–vis spectrometer (Epoch, BioTek) at 549 nm for RB and 620 nm for NB, respectively. The PQ was calculated by the ratio of the dye bound onto the NP surface to the free dye in the liquid phase. PQ versus surface area of the NPs was plotted, and the slope of the linear regression was obtained with OriginPro. The relative hydrophobicity is represented by the dye

adsorption ratio, calculated by the ratio of RB adsorption to NB adsorption, to eliminate uncertainties introduced when estimating the surface area of NPs.

RESULTS AND DISCUSSION

Characterization of the NPs. Figure 2 shows the electron micrographs of six representative NPs that cover a range of chemistries and morphologies. These are (A) triethoxycaprylsilane-coated zinc oxide (TCS-ZnO) NPs, (B) multiwalled carbon nanotubes (MWCNT), (C) titanium dioxide (TiO₂) NPs, (D) graphene nanoplatelets (GNP), (E) cerium oxide (CeO₂) NPs, and (F) polystyrene (PST) NPs. The source, morphology, primary and hydrodynamic sizes, ζ -potential, and measured SFE values of these NPs are summarized in Table 1.

Mechanisms of the MPD Method. The MPD method determines the SFE of NPs based on a novel measurement principle of controlling the colloidal stability of NP suspensions. According to classical DLVO theory, the work of adhesion between particles dispersed in a liquid medium depends on a balance between the repulsive electrostatic forces and the attractive van der Waals forces.² The Lifshitz theory predicts that the van der Waals attraction between alike particles, i.e., the Hamaker constant, is minimized when the SFE of the liquid medium (i.e., its surface tension) is equal to that of the particles.³⁰ Consequently, when dispersing particles in a series of liquid media with a range of surface tensions, e.g., a series of water/ethanol mixtures, the particles are expected to be maximally dispersed, or least agglomerated, in the liquid whose surface tension is the closest to that of the SFE of the

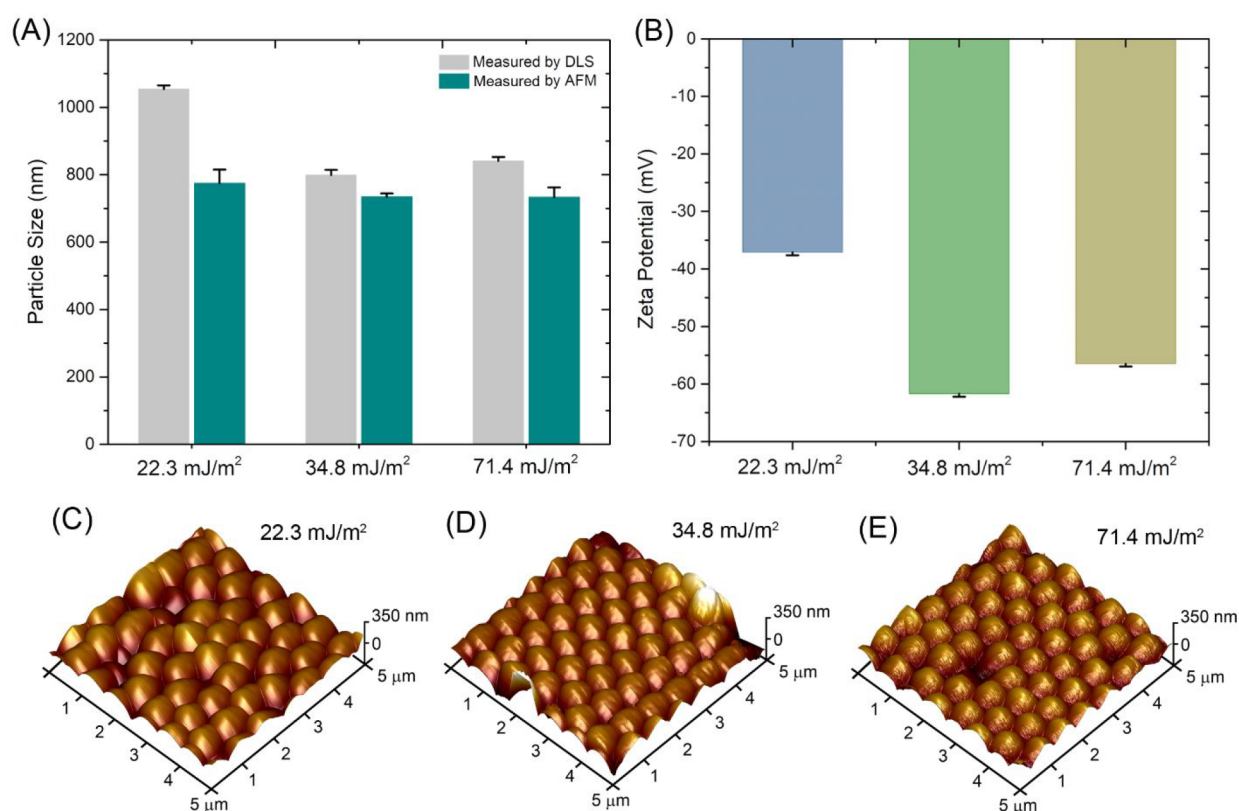


Figure 4. Aggregation state of PST NPs in three representative probing liquids, i.e., pure ethanol (22.3 mJ/m²), pure water (71.4 mJ/m²), and the ethanol/water mixture in which the PST NPs are maximally dispersed (34.8 mJ/m²). (A) Hydrodynamic size of the PST NPs determined with DLS and the particle size determined with AFM. (B) ζ -potentials of the PST NPs in three suspending liquids. (C–E) AFM topographic images of the PST NPs in three suspending liquids.

particles. The state of particle dispersion in a series of liquids can be readily compared by measuring light absorbance using a microplate reader. The surface tension of the liquid in which particles are maximally dispersed, i.e., with the highest optical density, is expected to be equal to the SFE of the suspending particles.

We first scrutinized the underlying mechanisms of the MPD method using two representative NPs, i.e., TiO₂ and PST NPs. These two NPs were selected due to their opposite charges when dispersed in liquid media consisting of water/ethanol mixtures. It should be noted that the ζ -potential of NPs is determined by their isoelectric point and the pH value of the dispersion liquid. The isoelectric points of TiO₂ and PST NPs are approximately 6 and 3.8, respectively.^{32–34} The literature values for the isoelectric points of all NPs used in this study are summarized in Table S2. When dispersed in the standard PBS solution at pH 7.4, both TiO₂ and PST NPs are negatively charged (Table 1). However, when dispersed in water/ethanol mixtures, although the PST NPs remain negatively charged (Figure 4B), the TiO₂ NPs appear to have a positive ζ -potential (Figure 3B). This charge transition for TiO₂ NPs dispersed in water/ethanol mixtures has been previously reported.^{35,36}

Figure 3 illustrates the aggregation state of TiO₂ NPs in three characteristic probing liquids, i.e., pure water and pure ethanol with surface tensions of 71.4 and 22.3 mJ/m², respectively, and the water/ethanol mixture with a surface tension of 30.4 mJ/m² in which the TiO₂ NPs are expected to be maximally dispersed. Figure S1 shows the size distribution of the TiO₂ NPs dispersed in these three probing liquids,

determined with DLS. It can be seen that TiO₂ NPs suspended in pure ethanol (22.3 mJ/m²) demonstrate a broader size distribution than those suspended in the mixture (30.4 mJ/m²) or in pure water (71.4 mJ/m²). The PDI of the TiO₂ NPs in ethanol was determined to be 0.208 ± 0.004, which is much larger than that in pure water (0.167 ± 0.020) or in the ethanol/water mixture (0.145 ± 0.020). The larger PDI and broader size distribution indicate significant particle aggregation/agglomeration in pure ethanol. Using cumulant analysis of the DLS results, Figure 3A shows that the average hydrodynamic size of TiO₂ NPs in the water/ethanol mixture is 202 ± 1 nm, in contrast to 310 ± 15 nm in pure ethanol and 210 ± 1 nm in pure water. Given the primary size of the TiO₂ NPs at 23 nm (Table 1), the particles indeed aggregate less in the mixture than in water or in ethanol.

To further verify the aggregation state of TiO₂ NPs dispersed in the probing liquids, we have directly examined their morphology using AFM. As shown in Figure 3C–E and Figure S2, TiO₂ NPs suspended in pure ethanol demonstrate more agglomeration than those in the mixture, in spite of the larger ζ -potential in ethanol (Figure 3B). In general, it is found that the particle sizes determined with AFM are smaller than those determined with DLS (Figure 3A). Nevertheless, both DLS and AFM measurements suggest that the TiO₂ NPs are less aggregated in the ethanol/water mixture than in pure water or in ethanol. Collectively, results from DLS and AFM support the principle and mechanism of the MPD method.

Figure 4 shows the aggregation state of PST NPs in pure water, ethanol, and the mixture in which the PST NPs are expected to be maximally dispersed. We found that the PST

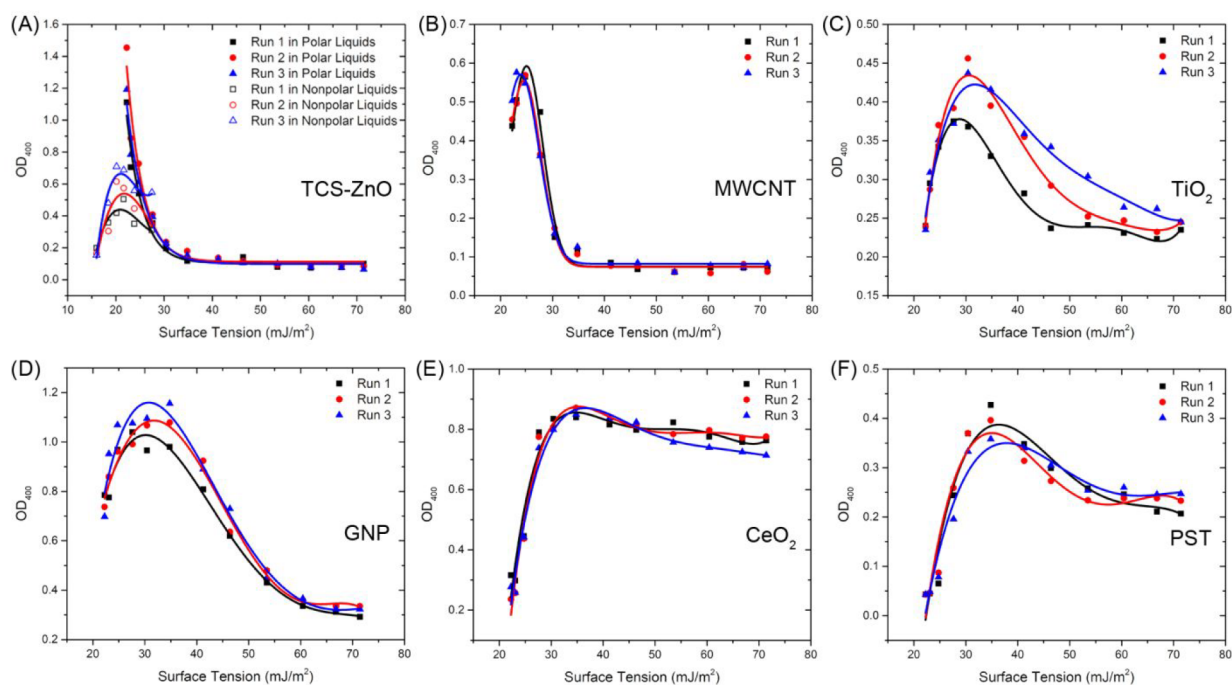


Figure 5. Quantitative determination of the SFE of NPs using the maximum particle dispersion (MPD) method: (A) TCS-ZnO NPs, (B) MWCNT, (C) TiO₂ NPs, (D) GNP, (E) CeO₂ NPs, and (F) PST NPs. Among these NPs, the TCS-ZnO NPs were studied with both polar (solid symbols) and nonpolar (open symbols) liquid sets, while the others were only studied with the polar probing liquids. Three runs of each measurement are presented to show reproducibility. The determined SFE values are summarized in Table 1.

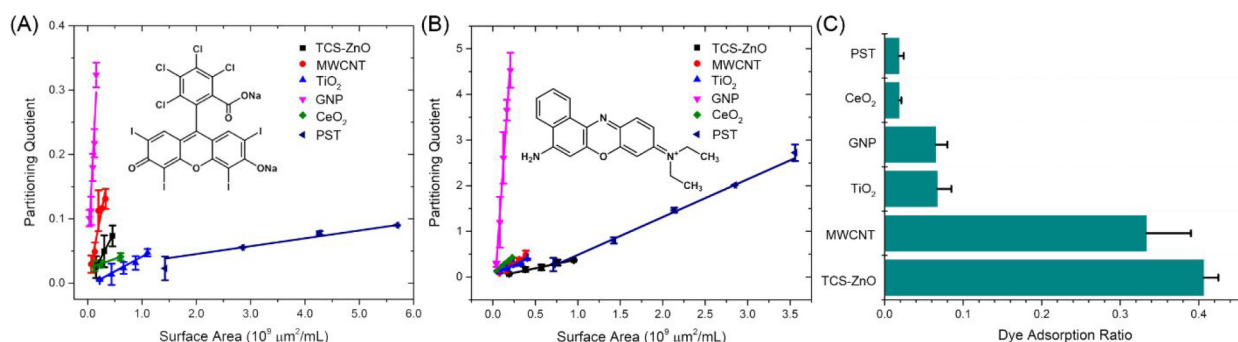


Figure 6. Qualitative determination of the hydrophobicity of NPs using the relative dye adsorption method. (A) Relative hydrophobicity of the NPs determined with Rose bengal (RB) partitioning. (B) Relative hydrophilicity of the NPs determined with Nile blue (NB) partitioning. (C) The RB/NB dye adsorption ratio as an indication of the relative hydrophobicity of these NPs.

NPs have an average size of 799 ± 15 nm in the mixture (34.8 mJ/m²), in contrast to 1054 ± 11 nm in pure ethanol and 841 ± 12 nm in pure water (Figure 4A and Figure S3). Given the primary and hydrodynamic sizes of these PST NPs at 707 and 803 nm, respectively (Table 1), the PST NPs in the mixture exist as well-dispersed individual particles without significant aggregation. The PDI of the PST NPs in the ethanol/water mixture was measured as 0.152 ± 0.049 , which is lower than that in ethanol (0.205 ± 0.007) or in pure water (0.186 ± 0.032).

The aggregation state of PST NPs was further studied with direct AFM observation (Figure 4C–E and Figure S4). Different from TiO₂ NPs, the PST NPs do not significantly agglomerate in all three studied liquids. Variations of the hydrodynamic size of the PST NPs in water, ethanol, and their mixtures may be explained by conformational transitions of the polymers. The conformation of PST NPs dispersed in liquids is determined by the interfacial free energy between the PST NPs

and the probing liquid.³⁷ When being dispersed in a poor solvent, the polymer chains of polystyrene are forced to solvate by the external force and are pulled out of the collapsed state into the solvent, resulting in a coexistence of the collapsed and extended states.^{37,38} With increasing ethanol content in the mixture, the interfacial free energy decreases and the collapsed–extended coexistence conformation transforms toward a fully extended conformation, thus increasing the hydrodynamic size of the PST NPs.^{37,38} The lack of significant aggregation in pure water makes the PST NPs settle at a similar speed as that in the mixture, thus resulting in an OD curve in an inverted L-shape (Figure 5F) rather than the bell shape observed for TiO₂ NPs (Figure 5C). Nevertheless, the OD measurements show a local peak that indicates the SFE of the dispersed particles.

Quantitative Hydrophobicity Measurements with the MPD Method. Figure 5 shows the SFE measurements of the six NPs with the MPD method, each with three repetitions.

When measured with the water/ethanol mixtures, the OD value of TCS-ZnO NPs monotonically increased with the reduction of surface tension from 71.4 to 22.3 mJ/m² as shown in Figure 5A. This indicated that the SFE of TCS-ZnO NPs falls into a range lower than the surface tension of ethanol, thus necessitating the use of a nonpolar liquid set that consists of six pure alkanes, i.e., pentane, hexane, heptane, octane, decane, and hexadecane, covering the surface tension range from 16 to 27 mJ/m². When measured with this nonpolar liquid set, an OD peak appears at 21.2 mJ/m², indicating maximum particle dispersion. The OD curves obtained with both the polar and nonpolar liquid sets collectively show that only a single peak can be determined at 21.2 ± 0.4 mJ/m² in a large surface tension range from 16 to 71.4 mJ/m², which is in good agreement with our previous measurements.³⁰ The other five NPs, i.e., MWCNT, TiO₂, GNP, CeO₂, and PST, were measured with only the polar liquid set, which provided a sufficiently large surface tension range to cover the SFE of these NPs (Figure 5B–F). The SFE values of these NPs are summarized in Table 1. On the basis of this quantitative characterization of SFE, the hydrophobicity of these six NPs is ranked as TCS-ZnO > MWCNT > TiO₂ ≈ GNP > CeO₂ ≈ PST.

Verification of the MPD Method. We further verified the MPD method by qualitatively determining the hydrophobicity of the NPs using a relative dye adsorption method that utilizes both the hydrophobic dye, RB,¹⁵ and the hydrophilic dye, NB.¹⁴ Figure 6, parts A and B, shows the PQ of RB and NB against the surface area of the NPs, where the slopes are proportional to the relative hydrophobicity and the relative hydrophilicity of the NPs, respectively. To eliminate the uncertainty in determining the surface area of the NPs, Figure 6C shows the dye adsorption ratio between RB and NB, which indicates the relative hydrophobicity of the studied NPs, ranking them as TCS-ZnO > MWCNT > TiO₂ ≈ GNP > CeO₂ ≈ PST. This rank is in excellent agreement with the SFE results of the NPs determined with the MPD method (Table 1). It should be noted that the SFE determined with the MPD method represents an absolute physicochemical property of the NPs, which enables standardization and comparison across literature. In contrast, the hydrophobicity ranking determined with the dye partitioning method is a relative measure of the NPs' hydrophobicity, which cannot be directly compared across literature.

Further Development of the MPD Method. Due to its simplicity in both experimental implementation and theoretical interpretation, the MPD method holds great promise to become a standard method for quantitatively determining the hydrophobicity of NPs. Nevertheless, the current MPD method still has limitations that require further development. A major limitation of the MPD method lies in the probing liquids used for dispersing NPs, i.e., water/ethanol mixtures. According to Stokes' law, the sedimentation velocity of particles in a liquid is not only dependent on the particles size (i.e., proportional to the radius square of the particles) but also on the physical properties of the liquid, i.e., proportional to the density difference between particles and the liquid, and inversely proportional to the viscosity of the liquid. As shown in Figure S5, with increasing ethanol fraction in water, the density of the mixture nearly linearly decreases, with a total reduction of less than 20% that of water. However, the viscosity of the water/ethanol mixture shows a peak at the ethanol mole fraction of 0.27, at which the viscosity of the

mixture more than doubles that of pure water or pure ethanol. Such a positive viscosity deviation in binary mixtures of water and an organic solvent, including ethanol, has been reported previously and is explained by the formation of ethanol micelles in water due to hydrophobic attractions.³⁹ Ethanol molecules possess a hydrophilic hydroxyl group and a hydrophobic alkyl group. Formation of micelles in pure ethanol is unfavorable due to steric repulsions between the alkyl groups. However, when mixed with water, the hydrophilic hydroxyl group of ethanol forms hydrogen bonds with water molecules, thus disrupting the highly ordered structure while promoting micelle formation through hydrophobic hydration.^{40,41} It is known that water in the hydration layer surrounding micelles is much more viscous than the bulk water, thus leading to the viscosity peak in the water/ethanol mixture (Figure S5).^{39,42} This positive viscosity deviation in the water/ethanol mixture could introduce artifacts into the MPD measurement if natural sedimentation within a limited time period was relied on to separate the aggregated NPs from the supernatant. At present, we partially circumvented this technical difficulty by using centrifugal sedimentation (100–700g for at least 5 min) instead of natural sedimentation.

Another potential problem associated with the water/ethanol mixtures being the probing liquids lies in the difficulty of controlling the electrostatic interactions across these polar liquid media. The measurement principle of the MPD method relies on the quantitative characterization of colloidal stability as a result of competition between the van der Waals attraction and electrostatic repulsion. It would be ideal to decouple these two opposing interactions, e.g., selectively varying the van der Waals attraction, by changing liquid media of various surface tensions but keeping the electrostatic repulsion constant or under control. However, as shown in Figure 3, this has been proven to be technically difficult since the polar probing liquids made of water/ethanol mixtures complicate the electrostatic interactions by varying the pH of the media and/or the ζ -potential of the NPs. We are now investigating a new set of nonpolar probing liquids using single or binary organic solvents, similar to the nonpolar liquid set shown in Figure S6 and Table S1 but with an extended surface tension range.

CONCLUSIONS

We have developed a novel optical method, called the maximum particle dispersion (MPD), for quantitatively characterizing the hydrophobicity of NPs. The measurement principle of the MPD method lies in controlling the aggregation state of the NPs, demonstrated with DLS and AFM, via manipulation of the van der Waals interactions between NPs across the dispersion liquid. It is shown that the MPD method is capable of determining the SFE of six representative NPs of various chemistries and morphologies. The hydrophobicity of these six NPs ranks as TCS-ZnO (21.2 mJ/m²) > MWCNT (24.5 mJ/m²) > TiO₂ (30.4 mJ/m²) ≈ GNP (30.9 mJ/m²) > CeO₂ (35.5 mJ/m²) ≈ PST (36.4 mJ/m²), which is in excellent agreement with results obtained from the relative dye adsorption method. The MPD method holds great promise to be developed into an easy-to-use, standard method for quantitatively characterizing the hydrophobicity of NPs.

■ ASSOCIATED CONTENT

SI Supporting Information

The Supporting Information is available free of charge at <https://pubs.acs.org/doi/10.1021/acs.analchem.1c04172>.

Particle size distribution of TiO₂ NPs determined with DLS, aggregation state of TiO₂ NPs determined with AFM, particle size distribution of PST NPs determined with DLS, aggregation state of PST NPs determined with AFM, physical properties of water/ethanol mixtures, physical properties of pure alkanes, summaries of liquids used for the MPD method, and the isoelectric points of NPs (PDF)

■ AUTHOR INFORMATION

Corresponding Author

Yi Y. Zuo – Department of Mechanical Engineering, University of Hawaii at Manoa, Honolulu, Hawaii 96822, United States; Department of Pediatrics, John A. Burns School of Medicine, University of Hawaii, Honolulu, Hawaii 96826, United States; orcid.org/0000-0002-3992-3238; Phone: 808-956-9650; Email: yzuo@hawaii.edu; Fax: 808-956-2373

Authors

Guangle Li – Department of Mechanical Engineering, University of Hawaii at Manoa, Honolulu, Hawaii 96822, United States

Zhenle Cao – Department of Mechanical Engineering, University of Hawaii at Manoa, Honolulu, Hawaii 96822, United States

Kacie K. H. Y. Ho – Department of Human Nutrition, Food and Animal Sciences, University of Hawaii at Manoa, Honolulu, Hawaii 96822, United States

Complete contact information is available at:

<https://pubs.acs.org/doi/10.1021/acs.analchem.1c04172>

Notes

The authors declare no competing financial interest.

■ ACKNOWLEDGMENTS

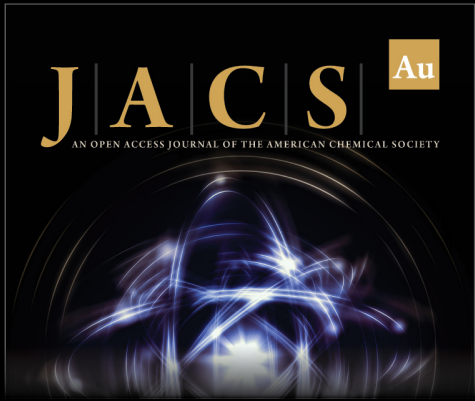
This research was supported by the National Science Foundation Grant No. CBET-2011317 (Y.Y.Z.).

■ REFERENCES

- (1) Neumann, A. W.; Robert, D.; Zuo, Y. *Applied Surface Thermodynamics*, 2nd ed.; CRC Press: Boca Raton, FL, 2010.
- (2) Israelachvili, J. *Intermolecular and Surface Forces*, 3rd ed.; Academic Press: Waltham, MA, 2011.
- (3) Nel, A. E.; Mädler, L.; Velegol, D.; Xia, T.; Hoek, E. M. V.; Somasundaran, P.; Klaessig, F.; Castranova, V.; Thompson, M. *Nat. Mater.* **2009**, *8* (7), 543–557.
- (4) Monopoli, M. P.; Åberg, C.; Salvati, A.; Dawson, K. A. *Nat. Nanotechnol.* **2012**, *7* (12), 779–786.
- (5) Olenick, L. L.; Troiano, J. M.; Vartanian, A.; Melby, E. S.; Mensch, A. C.; Zhang, L.; Hong, J.; Mesele, O.; Qiu, T.; Bozich, J.; Lohse, S.; Zhang, X.; Kuech, T. R.; Millevolte, A.; Gunsolus, I.; McGeachy, A. C.; Doğançün, M.; Li, T.; Hu, D.; Walter, S. R.; Mohaimani, A.; Schmoldt, A.; Torelli, M. D.; Hurley, K. R.; Dalluge, J.; Chong, G.; Feng, Z. V.; Haynes, C. L.; Hamers, R. J.; Pedersen, J. A.; Cui, Q.; Hernandez, R.; Klapper, R.; Orr, G.; Murphy, C. J.; Geiger, F. M. *Chem.* **2018**, *4* (11), 2709–2723.
- (6) Hu, Q.; Bai, X.; Hu, G.; Zuo, Y. Y. *ACS Nano* **2017**, *11* (7), 6832–6842.

- (7) Moyano, D. F.; Goldsmith, M.; Solfiell, D. J.; Landesman-Milo, D.; Miranda, O. R.; Peer, D.; Rotello, V. M. *J. Am. Chem. Soc.* **2012**, *134* (9), 3965–3967.
- (8) Dobrovolskaia, M. A.; McNeil, S. E. *Nat. Nanotechnol.* **2007**, *2* (8), 469–478.
- (9) Zhu, Z.-J.; Posati, T.; Moyano, D. F.; Tang, R.; Yan, B.; Vachet, R. W.; Rotello, V. M. *Small* **2012**, *8* (17), 2659–2663.
- (10) Lasagna-Reeves, C.; Gonzalez-Romero, D.; Barria, M. A.; Olmedo, I.; Clos, A.; Sadagopa Ramanujam, V. M.; Urayama, A.; Vergara, L.; Kogan, M. J.; Soto, C. *Biochem. Biophys. Res. Commun.* **2010**, *393* (4), 649–655.
- (11) Kuna, J. J.; Voitchovsky, K.; Singh, C.; Jiang, H.; Mwenifumbo, S.; Ghorai, P. K.; Stevens, M. M.; Glotzer, S. C.; Stellacci, F. *Nat. Mater.* **2009**, *8* (10), 837–842.
- (12) Feng, X.; Feng, L.; Jin, M.; Zhai, J.; Jiang, L.; Zhu, D. *J. Am. Chem. Soc.* **2004**, *126* (1), 62–63.
- (13) Jafvert, C. T.; Kulkarni, P. P. *Environ. Sci. Technol.* **2008**, *42* (16), 5945–5950.
- (14) Xiao, Y.; Wiesner, M. R. *Journal of Hazardous Materials* **2012**, *215–216*, 146–151.
- (15) Müller, R. H.; Rühl, D.; Lück, M.; Paulke, B. R. *Pharm. Res.* **1997**, *14* (1), 18–24.
- (16) Crandon, L. E.; Boenisch, K. M.; Harper, B. J.; Harper, S. L. *PLoS One* **2020**, *15* (6), e0233844.
- (17) Wang, S.; Zhang, Y.; Abidi, N.; Cabrales, L. *Langmuir* **2009**, *25* (18), 11078–11081.
- (18) Azimi, G.; Dhiman, R.; Kwon, H.-M.; Paxson, A. T.; Varanasi, K. K. *Nat. Mater.* **2013**, *12* (4), 315–320.
- (19) Alexander, S.; Eastoe, J.; Lord, A. M.; Guittard, F.; Barron, A. R. *ACS Appl. Mater. Interfaces* **2016**, *8* (1), 660–666.
- (20) Kwok, D. Y.; Neumann, A. W. *Adv. Colloid Interface Sci.* **1999**, *81* (3), 167–249.
- (21) Arnaudov, L. N.; Cayre, O. J.; Cohen Stuart, M. A.; Stoyanov, S. D.; Paunov, V. N. *Phys. Chem. Chem. Phys.* **2010**, *12* (2), 328–331.
- (22) Van Oss, C. J.; Chaudhury, M. K.; Good, R. J. *Chem. Rev.* **1988**, *88* (6), 927–941.
- (23) Grundke, K.; Augsburg, A. J. *Adhes. Sci. Technol.* **2000**, *14* (5), 765–775.
- (24) Mohammadi-Jam, S.; Waters, K. E. *Adv. Colloid Interface Sci.* **2014**, *212*, 21–44.
- (25) Das, S. C.; Larson, I.; Morton, D. A. V.; Stewart, P. J. *Langmuir* **2011**, *27* (2), 521–523.
- (26) Khodakarami, M.; Alagha, L.; Burnett, D. J. *ACS Omega* **2019**, *4* (8), 13319–13329.
- (27) Menzel, R.; Lee, A.; Bismarck, A.; Shaffer, M. S. P. *Langmuir* **2009**, *25* (14), 8340–8348.
- (28) Vargha-Butler, E. I.; Moy, A. W.; Neumann, E. *Colloids Surf.* **1987**, *24* (4), 315–324.
- (29) Valsesia, A.; Desmet, C.; Ojea-Jiménez, I.; Oddo, A.; Capomaccio, R.; Rossi, F.; Colpo, P. *Commun. Chem.* **2018**, *1* (1), 53.
- (30) Cao, Z.; Tsai, S. N.; Zuo, Y. Y. *Anal. Chem.* **2019**, *91* (20), 12819–12826.
- (31) Belda, R.; Herraes, J. V.; Diez, O. *Phys. Chem. Liq.* **2005**, *43* (1), 91–101.
- (32) Jing, C.; Meng, X.; Liu, S.; Baidas, S.; Patraju, R.; Christodoulatos, C.; Korfiatis, G. P. *J. Colloid Interface Sci.* **2005**, *290* (1), 14–21.
- (33) Suttiponparnit, K.; Jiang, J.; Sahu, M.; Suvachittanont, S.; Charinpanitkul, T.; Biswas, P. *Nanoscale Res. Lett.* **2011**, *6* (1), 27.
- (34) Bolt, P. S.; Goodwin, J. W.; Ottewill, R. H. *Langmuir* **2005**, *21* (22), 9911–9916.
- (35) Yu, J. C.; Jiang, Z.-T.; Liu, H.-Y.; Yu, J. J. *Colloid Interface Sci.* **2003**, *262* (1), 97–100.
- (36) Kosmulski, M.; Dahlsten, P.; Próchniak, P.; Rosenholm, J. B. Surface Charge and Conductance in Dispersions of Titania in Nonaqueous and Mixed Solvents. In *Trends in Colloid and Interface Science XXIV*; Starov, V., Procházka, K., Eds.; Springer: Berlin, Heidelberg, Germany, 2011; pp 55–59.

- (37) Li, I. T. S.; Walker, G. C. *J. Am. Chem. Soc.* **2010**, *132* (18), 6530–6540.
- (38) Banerjee, S.; Ghosh, R.; Bagchi, B. *J. Phys. Chem. B* **2012**, *116* (12), 3713–3722.
- (39) Song, S.; Peng, C. *J. Dispersion Sci. Technol.* **2008**, *29* (10), 1367–1372.
- (40) Akhtar, S.; Bhuiyan, M. M. H.; Uddin, M. S.; Meherun Nessa, B. S.; Saleh, M. A. *Phys. Chem. Liq.* **1999**, *37* (3), 215–227.
- (41) Grdadolnik, J.; Merzel, F.; Avbelj, F. *Proc. Natl. Acad. Sci. U. S. A.* **2017**, *114* (2), 322–327.
- (42) Tanaka, Y.; Matsuda, Y.; Fujiwara, H.; Kubota, H.; Makita, T. *Int. J. Thermophys.* **1987**, *8* (2), 147–163.



JACS Au
AN OPEN ACCESS JOURNAL OF THE AMERICAN CHEMICAL SOCIETY

 Editor-in-Chief
Prof. Christopher W. Jones
Georgia Institute of Technology, USA

Open for Submissions 

pubs.acs.org/jacsau  ACS Publications
Most Trusted. Most Cited. Most Read.